CORA Cork Open Research Archive
Cartlann Taighde Oscailte Chorcaí

Title	Enhanced thermoelectric properties of electrodeposited Cu-doped Te films
Authors	Lal, Swatchith;Razeeb, Kafil M.;Gautam, Devendraprakash
Publication date	2020-04-02
Original Citation	Lal, S., Razeeb, K. M. and Gautam, D. (2020) 'Enhanced thermoelectric properties of electrodeposited Cu-doped Te films', ACS Applied Energy Materials, 3(4), pp. 3262-3268. doi: 10.1021/acsaem.9b02153
Type of publication	Article (peer-reviewed)
Link to publisher's version	10.1021/acsaem.9b02153
Rights	© 2020, American Chemical Society. This document is the Accepted Manuscript version of a Published Work that appeared in final form in ACS Applied Energy Materials after technical editing by the publisher. To access the final edited and published work see https://pubs.acs.org/doi/abs/10.1021/acsaem.9b02153
Download date	2024-04-19 02:36:03
Item downloaded from	https://hdl.handle.net/10468/10489

UCC
University College Cork, Ireland
Coláiste na hOllscoile Corcaigh

Enhanced thermoelectric properties of electrodeposited Cu-doped Te films

Swatchith Lal, Kafil M. Razeeb[*] and Devendraprakash Gautam[*]

Micro-Nano Systems Centre, Tyndall National Institute, University College Cork, Lee Maltings, Dyke Parade, Cork T12 R5CP, Ireland

KEYWORDS: Thermoelectric material, Electrodeposition, Power-factor, Energy harvesting, Cu-doped Te thin films

ABSTRACT: Bismuth telluride based alloys are the best known thermoelectric materials in the room-temperature regime. Here, we report on the enhanced thermoelectric properties of electrodeposited copper doped tellurium films as n-type thermoelectric material for near room temperature applications. With increase of the copper content in the films, we observe an enhancement of the thermoelectric properties. Thereby, we investigate the role of copper in modifying the crystal structure, which leads to the amorphous nature of the films and the corresponding enhancement in the thermoelectric properties. The electrodeposited copper doped tellurium films exhibit a high Seebeck coefficient of -227 μV/K, resulting to a power factor of 5.6 mW/mK^2, which is a promising power factor observed for the electrodeposited thermoelectric materials and can be a favourable n-type thermoelectric material for device applications.

1. INTRODUCTION

The advancement in electronics and the constant drive for miniaturization has given rise to a highly integrated system but opened-up the challenge of managing the thermal budget of these integrated systems. Simultaneously, in the era of IoT[1-4] low power consuming wireless sensor nodes (typically in range of milli to micro watts) that enables to create a more smart and responsive environment are required. Typically, batteries employed to power-up these sensor nodes fail and need to be replaced after a limited time, which adds up to the cost.[3, 5] Therefore, power generation from abundant waste heat through thermoelectric (TE) materials is receiving huge attention by researchers both in academia and industry.[6, 7] A TE device can transform thermal energy into electricity using the "Seebeck effect" and conversely to enable cooling or heating using the "Peltier effect". Microscale TE devices have huge advantages over macroscopic devices. The apparent advantage is the smaller size, which allows integration into compact smaller systems. Due to the use of small structures, the integration density increases, thereby significantly increasing the number of thermocouples in the device leading to high power outputs, especially for small temperature differences.[8, 9] The present state of the art micro-thermoelectric generators (μTEG) are mainly fabricated using silicon fabrication technology and micro-electromechanical systems (MEMS) compatible techniques. These techniques are the basis of many rapidly growing technologies because they combine miniaturised sensors and actuators with electronics resulting in a substantial reduction in the device cost.[10, 11]

Another challenge to address is to synthesize highly efficient thermoelectric material. Bi_2Te_3 based thermoelectric materials still dominate the room temperature applications.[12-15] However, copper-based TE materials such as copper selenide,[16] copper sulphide[17, 18] and copper telluride[19] are getting renewed attention[20] as they exhibit excellent TE efficiency. It is worth mentioning that all

these copper-based TE materials are bulk materials exhibiting a p-type behaviour, and their working temperature are around ~700-900 K.[20] So far, all Cu-based thermoelectric materials reported in the literature demonstrated high TE performance at the high-temperature regime. Here, we report the development of Cu doped Te films for thermoelectric applications near room temperature. We synthesize Cu doped Te films using electrodeposition and characterise structural and TE properties of the as-deposited materials. The role of Cu on the crystal structure of the Te film and its effect on the thermoelectric properties are discussed in detail. The excellent thermoelectric properties exhibited by Cu doped Te films can lead to a potential thermoelectric material for power generation in near room temperature applications, specifically for low differential temperature scenarios.

A great deal of work in enhancing the ZT of the material has been carried out and reported in the literature over the last decade.[21-25] The maximum power density of a thermoelectric device is closely associated with the power factor of the thermoelectric materials. Higher power factors lead to larger output power densities for a given working condition.[26, 27] Developing thermoelectric materials with high power factor is crucially important for real-time applications. Here, we also report the extraordinary power factor exhibited by Cu doped Te film for room-temperature application which is at par with the highest power factor reported for thin-film thermoelectric material developed by electrodeposition so far.[28-30]

2. EXPERIMENTAL SECTION

All the depositions were performed at room temperature from an electrolyte containing 1 M nitric acid, 15 mM pure tellurium powder and 2 mM copper (II) sulphate pentahydrate. In order to prepare the solution, tellurium was first dissolved in 1 M nitric acid and heated at 40 °C while

stirring. Copper (II) sulphate pentahydrate was separately dissolved in de-ionised (DI) water. Both the solutions were mixed at a later stage while stirring to form the final solution. Cyclic voltammetry (CV) was performed using a standard gold electrode with respect to Ag/AgCl reference electrode at a sweep rate of 10 mV s^{-1}. Platinised titanium mesh was used as the counter electrode. The thermoelectric films were electrodeposited on Si/SiO_2 substrate, having 20 nm of gold (Au) layer on top of 10 nm titanium (Ti) adhesion layer. All the depositions were performed for 1 hour at room temperature by applying different deposition potentials (-50 to -250 mV). The deposition area of the sample was fixed to 9 cm^2. All the samples were rinsed using DI water and with isopropanol and again with DI water, before drying under nitrogen jet.

Morphology of the films was observed using scanning electron microscopy (SEM) (Quanta FEG 450) and the composition was determined with the energy-dispersive X-ray spectroscopy (EDS) attached to the SEM. The crystal orientation of the electrodeposited samples was studied using X-ray diffraction system (Pan analytical X'pert pro) with Cu K_α radiation (α=1.5406 Å) at a voltage of 40 kV and a current of 40 mA. The Raman spectra of the samples were recorded with the Renishaw (RA100) inVia confocal Raman microscope at 514.5 nm excitation.

The electrical transport and Hall properties were measured in the Van-der-Pauw arrangement at room temperature under a magnetic field of 1.7 T on 10×10 mm^2 thin film samples by using a Hall Kit (Lakeshore model 8404). The Hall measurements are of above 99% accuracy. For the Seebeck coefficient measurements; a laboratory built system was used. All the measurements were done in the in-plane orientation with different temperature gradients (ΔT), established along the ends of the samples using commercially available Peltier modules. The thermovoltage of the sample was measured over a range of ΔT values (2-10 °C), where the temperature was monitored using two separate thermocouples situated on either end of the sample. The Seebeck coefficient was

determined from the slope of the thermovoltage versus the temperature gradient. The measurement error is no more than 5% for this setup. Further details on the Seebeck coefficient measurements are provided in the Supporting Information section. The presence of Au seed layer underneath the deposited film and its impact on the thermoelectric and electrical property measurements of the film has been taken into consideration. However, telluride-based chalcogenides, such as BiTe alloys demonstrate anisotropic behaviour with respect to thermal/electrical properties.[31, 32] Hence, we think that it might be possible that the in-plane electrical resistivity is different compared to the cross-plane resistivity of the deposited material. The electrical resistivity was measured using an in-line four-point probe measurement system (Jandel RM3000), which was also used to cross-check the sheet resistance values obtained from the Hall measurements. The electrical conductivity values from both the techniques were almost the same, within an error of 4%.

3. RESULTS AND DISCUSSION

3.1 Electrochemical deposition

Electrolytic behaviour of different baths was investigated using CV to understand the reduction mechanism of the electrolyte with Cu and Te ions. Three separate baths were prepared, the first bath with 2 mM copper (II) sulphate pentahydrate dissolved in 200 ml DI water. The second bath consisting of 15 mM tellurium in 1 M nitric acid and the third bath with 2 mM copper (II) sulphate and 15 mM of tellurium in 1 M nitric acid. All the CV's were recorded using the standard gold electrode with respect to the Ag/AgCl reference electrode. Figure 1 shows the recorded CV's of the prepared baths. The CV from pure Cu bath depicts two cathodic and two anodic peaks, representing different reduction and oxidation states of Cu. One small and a broad reduction peaks are observed, with maximum current density at -40 mV and -217 mV respectively. The former

peak is due to the reduction of Cu^{2+} to Cu^{1+}, and the latter is due to the reduction of Cu^{1+} to metallic Cu^0 [33-35]. The two oxidation peaks correspond to Cu^{1+} and Cu^{2+} respectively.

$$Cu^{2+} + e \rightarrow Cu^{1+} \text{ (slow)} \quad (1)$$

$$Cu^{1+} + e \rightarrow Cu \text{ (fast)} \quad (2)$$

Dissolution of Te in the nitric acid gives rise to $HTeO_2^+$ ions, and the recorded CV of the bath has a single broad reduction peak with peak current at -180 mV resulting in the reduction of Te as depicted in equation (3) and single oxidation peak at 510 mV.

$$HTeO_2^+ + 4e^- + 3H^+ \rightarrow Te + 2H_2O \quad (3)$$

The CV recorded for the solution with 2 mM Cu and 15 mM Te in 1 M HNO_3, revealed a single broad peak at less negative potentials, with the maximum cathodic current at -70 mV as depicted in Figure 1. The CV also reveals the oxidation peak at 510 mV and an overlapping shoulder peak corresponding to the oxidation of Te and Cu respectively.

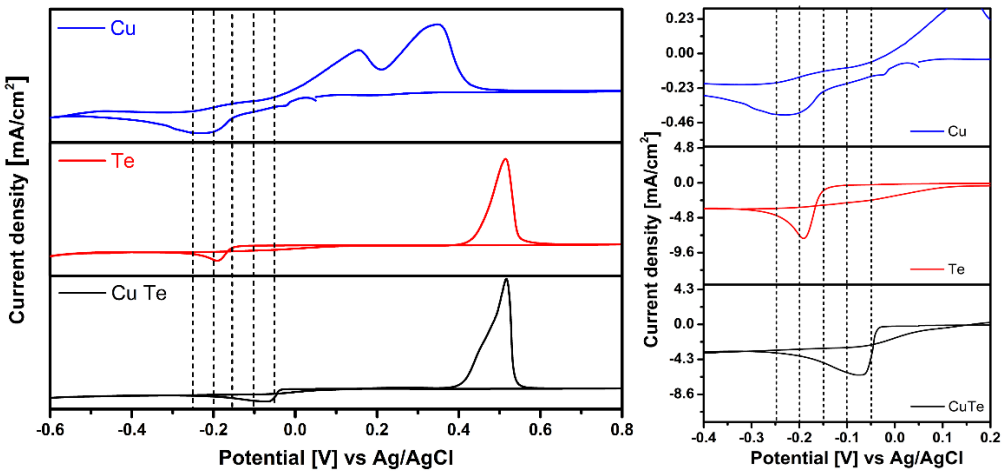

Figure 1. Cyclic voltammogram recorded on a standard gold working electrode in the Cu, Te, CuTe electrolyte and magnified image of reduction peaks (right).

Five different potentials were selected in order to understand the role of the deposition potential on the stoichiometry of the films. All the films were deposited at a constant potential ranging from -50 to -250 mV with an interval of -50 mV.

The elemental composition of the films deposited at different potentials is shown in Figure 2(a). The composition of the films varied with different deposition potentials as depicted in the figure. The film deposited at -50 mV led to maximum Cu percentage in the films of 16.06 %. Moreover, with an increase in the deposition potentials, Cu content tends to decrease to 6.45% for the films deposited at -150 mV. On further increasing the deposition potential (at -200 mV), Cu content increases and reaches to 11.94%. However, deposition at -250 mV resulted in a decrease in the Cu percentage as observed from EDS studies. This can be attributed to the Cu^{1+} reduction at a lower potential, leading to a higher Cu content in the films. Similarly, the reduction of Cu^{2+} ions to Cu is prominent at -200 mV, increasing the Cu reduction kinetics, thereby resulting in higher Cu content. However, Te maintains to be at significantly higher atomic percentages in the deposited films due to the higher ion concentration (15 mM) in the bath as compared to Cu with 2 mM concentration and due to higher reduction current of Te as can be observed in Figure 1.

Figure 2(b) shows the detrimental effect on the deposition rate with increase in the Cu content in the films. The films with less Cu have a higher deposition rate as compared to the films with the higher atomic percentage of Cu. This shows that the Cu content in the film hinders the kinetics of the film growth, resulting in a decrease in the deposition rates. This can be due to the formation of higher nucleation site of Cu hindering the deposition of Te.

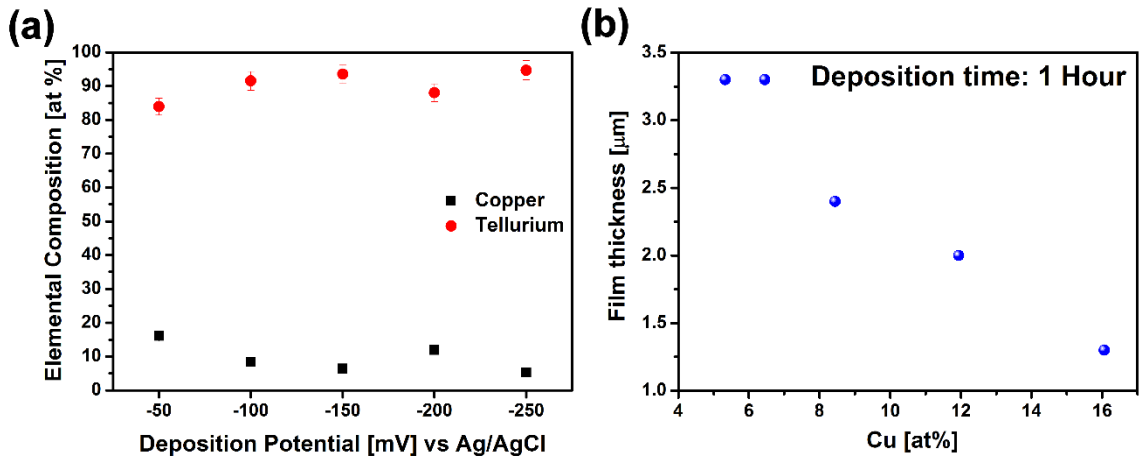

Figure 2. (a) Elemental composition of films at different deposition potentials and (b) The thickness of electrodeposited films with different Cu%.

3.2 STRUCTURAL PROPERTIES

The micrographs of the films deposited at different deposition potentials were recorded as shown in Figure 3. From the micrographs, we can see that there is no significant microstructure, revealing smooth and dense films. The films deposited at -100 mV, -150 mV and -250 mV, which also tend to have a Cu at. % of 8.44, 6.45 and 5.33, respectively have a solid and visibly flat structure. However, there is no structure observed for the other films deposited at -50 and -200 mV that have a higher Cu content of 16.06% and 11.94% as compared to the films deposited at other potentials. This study reveals that the Cu percentage in the films has a significant impact on the microstructure. To investigate further, a through TEM analysis was performed on the sample with maximum Cu content at multiple places. TEM showed a highly amorphous structure with no crystallite features, as shown in Figure 3(f). The selected area diffraction (SAED) rings further confirms that the films are amorphous as can been seen in Figure 3(f) inset. However, very few places in the sample showcased nano-features with no specific shapes. SAED was performed on

these features. As expected these features tend to be crystalline, and this is due to the presence of $Cu_{2-X}Te$ phase, confirmed using SAED as shown in the inset of Figure 3(g). In order to further investigate, X-ray diffraction (XRD) patterns of the films with increasing Cu at. % are plotted as shown in Figure 4.

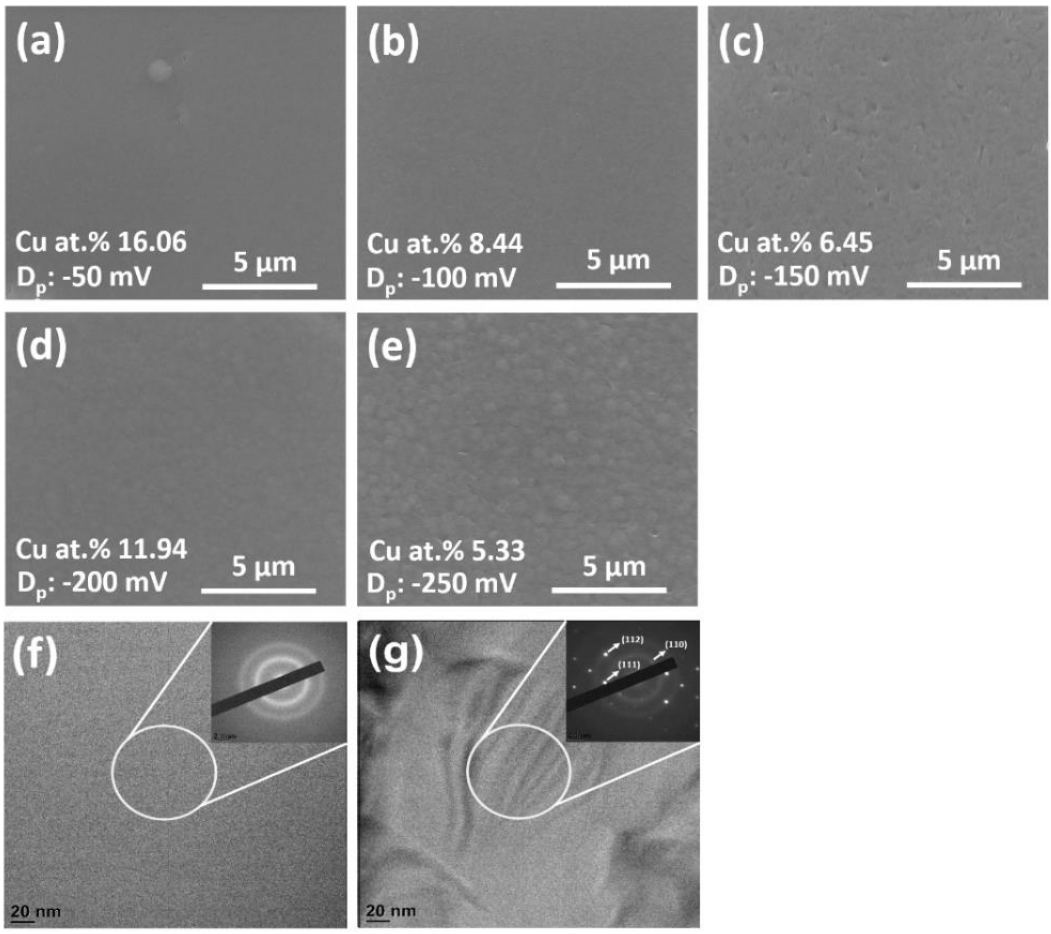

Figure 3. SEM and TEM micrographs of Cu doped Te films (a) -50 mV, (b) -100 mV, (c) -150 mV, (d) -200 mV, (e) -250 mV, (f) TEM image of the film deposited at -50 mV with SAED inset and (g) TEM image of the film deposited at -50 mV showing nano features along with SAED inset.

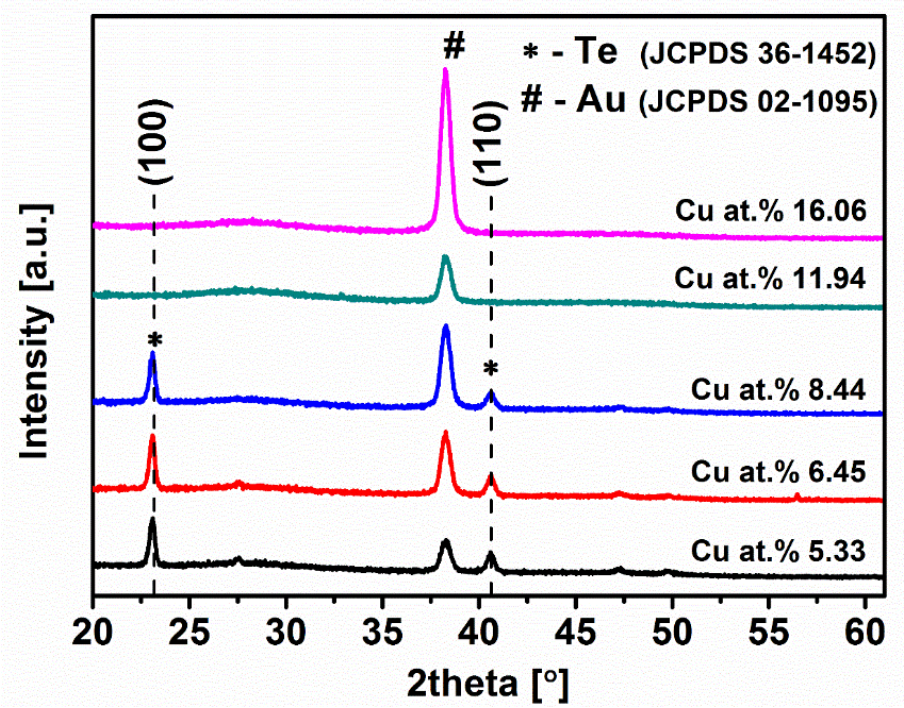

Figure 4. X-ray diffraction patterns of the deposited films with increasing Cu at. % in the films.

Table 1: Average crystallite size of the films with increasing Cu% in the films.

Copper [at. %]	**Deposition potential [mV]**	**Average crystallite size [nm]**	
		(100)	**(110)**
5.33	-250	26.45	20.10
6.45	-150	26.45	19.66
8.44	-100	25.65	17.01
11.94	-200	Amorphous	Amorphous
16.06	-50	Amorphous	Amorphous

Diffraction peaks of (100) and (110) are found for the films with Cu at.% < 11.94, and the observed diffraction peaks are indexed to a trigonal phase of tellurium (JCPDS 36-1452). The (100) diffraction peak located at 23.09, is the prominent peak for the films with Cu at% of 5.33%, 6.45% and 8.44%, and the peak at 2θ = 40.60 corresponds to the (110) crystallographic orientation. The Au diffraction peak (111) at 2θ = 38.25 originates due to the Au seed layer used for the electrodeposition of the films. Even though the EDS shows a substantial presence of Cu in the films, the XRD patterns show no pattern of either elemental Cu or CuTe phases. However, with an increase in the Cu percentage above 8.44% in the film, the crystal structure drastically collapsed as no diffraction peaks are observed for the films, and changing the films from crystalline to amorphous. The average crystallite size of different orientations was calculated using the Debye-Scherrer equation and shown in Table 1. With increase of the Cu content in the films until 8.44%, no major change in the average crystallite size is observed for the peak with (100) orientation. However, the crystallite size evaluated using (110) orientation decreased with an increase of Cu percentage in the film and finally the films became amorphous.

Raman spectra were recorded using a Renishaw (RA100) with an excitation wavelength of 514 nm at 50× magnification at different positions on the films. The Lorentzian function was used to fit the spectra and to obtain the peak value. The spectra were recorded at different spots of the films to ensure the reproducibility. There was no change in the peak positions with measurements done at different spots on the films, except a nominal difference in the intensities. The Raman spectra were recorded for different concentrations of Cu in Te films as shown in Figure 5. Three prominent Raman peaks are observed at ~92 cm^{-1}, ~122 cm^{-1} and 140 cm^{-1}. The Raman spectra for the Cu-doped Te films matches with the spectrum of Te thin films [36]. However, the spectra do not match with $Cu_{2-x}Te$ films [37, 38], confirming no $Cu_{2-x}Te$ phase formation and is in agreement

with our XRD data. The characteristic vibrational modes of different Te films from the literature and the films deposited in the present work are tabulated in Table 2.

Table 2: Tellurium vibrational modes measured in comparison with the data published in the literature.

Sample	Vibrational modes (cm^{-1})			Reference
	E^1	A^1	E^2	
Cu doped Te film	92	121.4	139.9	This work
Te cluster	93	123	142	[37]
1-D Te	94	122	142	[39]
Te film	88	117	137	[40]
Te film	91.3	119.7	139.5	[36]

As observed from Table 2, the Raman shift of tellurium films grown with different techniques has a spread in the recorded data. The most intense peak is located at ~122 cm^{-1}, which can be attributed to A^1 mode, corresponding to the chain expansion mode where each atom moves in the basal plane [39, 41]. Meanwhile, there exist two degenerate E modes, which separate into predominately bond-bending and bond-stretching types. E^1 mode at ~92 cm^{-1} is caused by a-axis rotation, and E^2 mode at ~140 cm^{-1} is attributed to asymmetric stretching mainly along the c-axis[41] as depicted in Figure 5. In order to study the effect of Cu addition in Te films, the shift in the Raman peaks is plotted with respect to the Cu concentration in the films (Figure 5(b)). With the addition of Cu, the prominent A^1 peak moves to higher Raman shift, till the Cu concentration reaches 8.44% and does not change for 11.94% Cu sample. In-between these Cu concentrations, there is a transformation from the crystalline to amorphous phase as observed from the XRD data

(see Figure 4). Further addition of Cu in the films reduces the Raman peak shift. A similar trend is followed by all other vibration modes, as can be seen in Figure 5(b). This shift to a higher frequency of Raman peak positions for Cu doped samples (as compared to pure Te) shows that Cu interacts with the Te chemical bonds, which finally results in collapsing of the crystal structure. From our XRD studies, it is clear that the addition of Cu distorts the crystal structure and after a particular concentration, the crystallinity diminishes with films getting amorphous. However, the mechanism of how Cu initiate and participate in the crystal distortion and finally collapsing the crystal structure without forming any separate phase with Te is still not clear. Nevertheless, this amorphous nature of the material has a significant impact on the thermoelectric properties as discussed in the subsequent section.

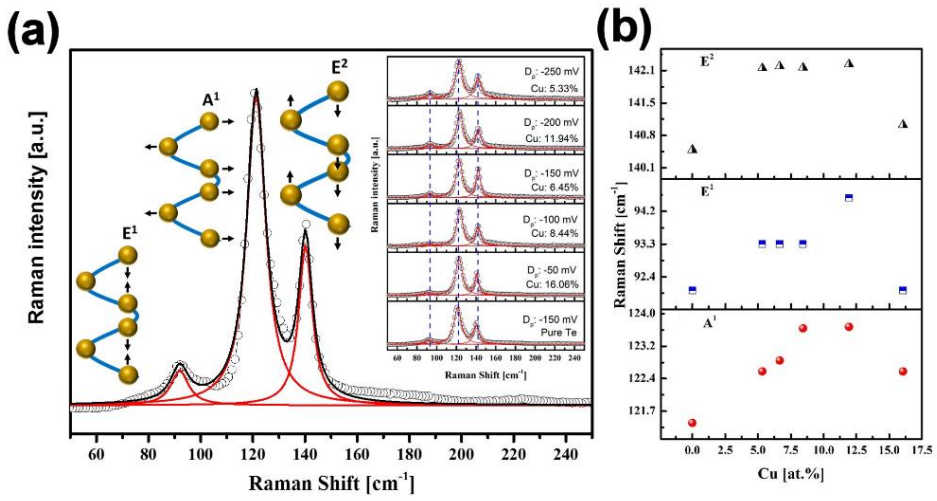

Figure 5. (a) Room temperature Raman scattering spectra of films without and with increasing Cu % in the films and (b) Raman spectra peak shift of A1, E1 and E2 peaks.

3.3 THERMOELECTRIC PROPERTIES

The thermoelectric properties of the electrodeposited films are investigated as a function of Cu concentration. Figure 6(a) shows the Seebeck coefficient and the electrical conductivities with

respect to Cu at% in the films. As discussed in the previous section, Cu content in the film changes with the deposition potentials. This change in Cu content has a direct impact on the thermoelectric properties of the electrodeposited films. The Seebeck coefficient of the films decreased with increase in the Cu content in the films except for the films deposited at -50 mV, which also tend to have maximum Cu content in the films. The film with the maximum Cu content of 16.06 at.% has a Seebeck coefficient of -227 μV/K.

The electrical conductivity of the films increased with increase of the Cu concentration in the films as shown in Figure 6(a). Addition of Cu enhances the electrical conductivity of the electrodeposited films with the maximum conductivity achieved by films with 16.06 at.% of Cu. In order to understand the impact of Cu content on thermoelectric properties of the films, electronic transport properties, carrier concentration and mobility were measured using a Hall probe. All the measured Hall voltages were negative in sign, indicating electrons as the majority charge carriers and confirming the negative Seebeck coefficient. Interdependent relation between the Seebeck coefficient, the carrier densities, the mobility and the electrical conductivity can be expressed by the following equations:

$$S = \frac{8\pi^2 k_b^2}{3eh^2} . m^* T \left(\frac{\pi}{3n}\right)^{\frac{2}{3}} \quad (4)$$

$$\frac{1}{\rho} = e . n . \mu \quad (5)$$

where n is the carrier density, k_b is the Boltzmann constant, e is the electron charge, h is the Planck constant, m^* is the charge carrier effective mass and μ is the mobility [14]. Electrical resistivity (ρ) of the film can be decreased with high carrier concentrations as well as with an increase in the carrier mobility as expressed in Eq. 5.

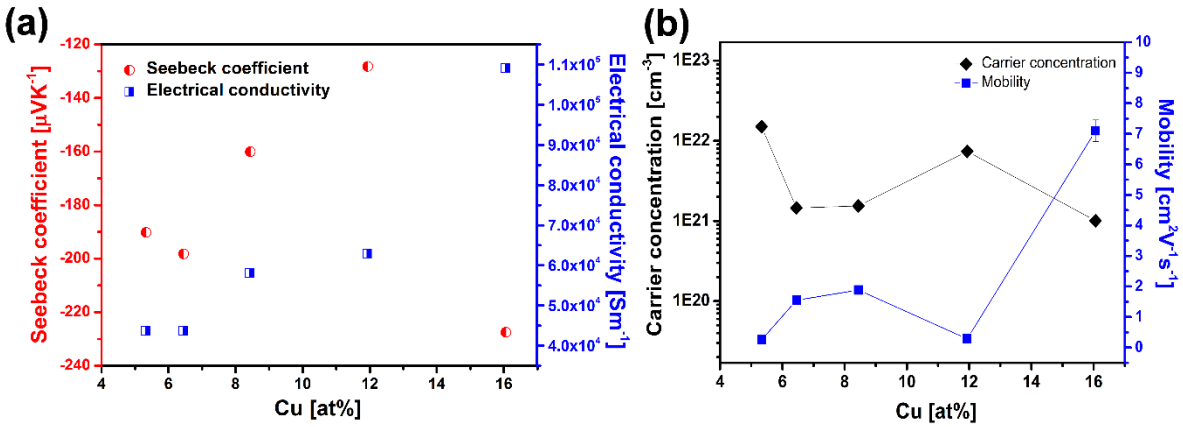

Figure 6. (a) Thermoelectric properties of electrodeposited Cu doped Te films with different Cu content in the films and (b) Mobility and carrier concentration as a function of Cu percentage in the films.

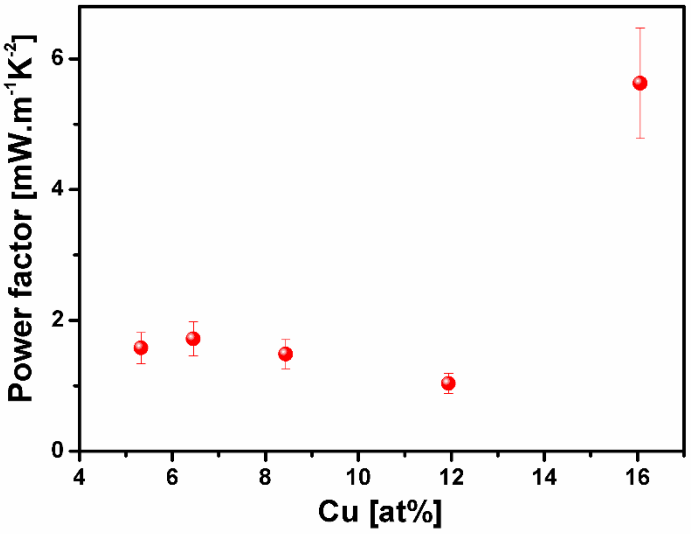

Figure 7. The calculated power factor of the films with different Cu% in the films.

The change in the carrier concentrations and the mobility of the films can be directly correlated with the Seebeck and electrical conductivities of the films with different Cu concentrations. Figure 6(b) shows carrier concentration and mobility as a function of Cu concentration in the films. The mobility of the films initially increases from 0.25 – 1.8 $cm^2V^{-1}s^{-1}$ for the films with 5.33 to 8.44% Cu. On further increase in the Cu content, at which the crystallinity of the films collapses, a sudden

decrease in the mobility to 0.28 $cm^2V^{-1}s^{-1}$ can be observed for the films with 11.94% Cu content. This decrease in mobility might have a direct relation with the collapse in crystallinity of the films. However, a further increase in Cu content (16.06%) resulted in maximum mobility of 7.1 $cm^2V^{-1}s^{-1}$. The presence of nano-crystalline features in the sample with Cu content of 16.06 at. % as observed in the TEM analysis shown in the Figure 3(g) might be the reason for an increase in the mobility, which ultimately increased the overall electrical conductivity of the sample. On the other hand, the charge carrier concentration of the films does not show any drastic change as a function of Cu content in the films and stays within the range of 10^{21}-10^{22} cm^{-3}. The film with maximum Cu content exhibits the lowest charge concentrations, which leads to high Seebeck coefficient values for the films.

The overall increase in the Seebeck coefficient and the electrical conductivity resulted in high power factors of Cu doped Te films at room temperature. The films with the Cu content of ~5 – 12 at. % have a power factor of ~1-1.7 mW/mK^2 and the film with a high percentage of Cu showed a maximum power factor of 5.6 mW/mK^2 as shown in Figure 7, which is highest power factor obtained for an electrodeposited near-room temperature thermoelectric material. In comparison with thermoelectric materials synthesized using other deposition techniques, the obtained power factor of the Cu doped Te electrodeposited films stands out not only with Bi-Te based thermoelectric materials but also with the CrN thin films which have shown promising thermoelectric performance near room-temperature recently.[30, 42] Further investigation on the temperature dependence of the thermoelectric properties of the deposited films are required to evaluate its application in future micro-thermoelectric devices for wider temperature range applications.

4. CONCLUSIONS

Cu-doped Te films with varying Cu content were electrodeposited using different reduction potentials. Reduction of Cu, Te and CuTe were studied using cyclic voltammetry. The Cu content has a significant impact on the structure of the electrodeposited films as well as on its thermoelectric performance. Increase of the Cu content over a certain range tends to destroy the crystallinity of the films and eventually making them amorphous. The as-deposited films show an n-type behaviour with a maximum Seebeck coefficient of -227 μV/K resulting in a power factor of 5.6 mW/mK^2, which is one of the most promising power factor values as compared to the reported contemporary electrodeposited room-temperature thermoelectric material.

SUPPORTING INFORMATION

Seebeck coefficient measurement setup and working principle; raw data of the thermovoltage vs. temperature gradient of the electrodeposited samples; re-measurement of the -50 mV deposited sample eight months after the film deposition; RMS roughness analysis on the films using AFM measurements; reproducibility study of the -50 mV deposited sample.

AUTHOR INFORMATION

Corresponding Authors

*E-mail: kafil.mahmood@tyndall.ie

*E-mail: gautam3000in@gmail.com

Funding Sources

This work has received funding from the European Union's Horizon 2020 funded project under grant agreement No. 825114 (SmartVista). Authors also acknowledge support by Science Foundation Ireland (SFI) through SFI grants 15/IA/3160 and 12/RC/2276.

REFERENCES

1. Du, L.; Shi, G.; Zhao, J., Review of micro magnetic generator. *Sens Transducers* **2014,** *176*, 1-12.

2. Calhoun, B. H.; Daly, D. C.; Naveen, V.; Finchelstein, D. F.; Wentzloff, D. D.; Wang, A.; Seong-Hwan, C.; Chandrakasan, A. P., Design considerations for ultra-low energy wireless microsensor nodes. *IEEE Transactions on Computers* **2005,** *54* (6), 727-740.

3. Haras, M.; Skotnicki, T., Thermoelectricity for IoT – A review. *Nano Energy* **2018,** *54*, 461-476.

4. Rabaey, J. M.; Ammer, J.; Karalar, T.; Suetfei, L.; Otis, B.; Sheets, M.; Tuan, T. In *PicoRadios for wireless sensor networks: the next challenge in ultra-low power design*, 2002 IEEE International Solid-State Circuits Conference. Digest of Technical Papers (Cat. No.02CH37315), 7-7 Feb. 2002; 2002; pp 200-201 vol.1.

5. Arnold, D. P., Review of Microscale Magnetic Power Generation. *IEEE Transactions on Magnetics* **2007,** *43* (11), 3940-3951.

6. Selvan, K. V.; Mohamed Ali, M. S., Micro-scale energy harvesting devices: Review of methodological performances in the last decade. *Renewable and Sustainable Energy Reviews* **2016,** *54*, 1035-1047.

7. Dahiya, A. S.; Thireau, J.; Boudaden, J.; Lal, S.; Gulzar, U.; Zhang, Y.; Gil, T.; Azemard, N.; Ramm, P.; Kiessling, T.; O'Murchu, C.; Sebelius, F.; Tilly, J.; Glynn, C.; Geary, S.; O'Dwyer, C.; Razeeb, K. M.; Lacampagne, A.; Charlot, B.; Todri-Sanial, A., Review—Energy Autonomous Wearable Sensors for Smart Healthcare: A Review. *Journal of The Electrochemical Society* **2020,** *167* (3).

8. Fleurial, J. P.; Snyder, G. J.; Herman, J. A.; Giauque, P. H.; Phillips, W. M.; Ryan, M. A.; Shakkottai, P.; Kolawa, E. A.; Nicolet, M. A. In *Thick-film thermoelectric microdevices*, Thermoelectrics, 1999. Eighteenth International Conference on, Aug. 29 1999-Sept. 2 1999; 1999; pp 294-300.

9. Lal, S.; Gautam, D.; Razeeb, K. M., Fabrication of micro-thermoelectric devices for power generation and the thermal management of photonic devices. *Journal of Micromechanics and Microengineering* **2019,** *29* (6), 065015.

10. Snyder, G. J.; Lim, J. R.; Huang, C.-K.; Fleurial, J.-P., Thermoelectric microdevice fabricated by a MEMS-like electrochemical process. *Nat Mater* **2003,** *2* (8), 528-531.

11. Dunham, M. T.; Barako, M. T.; LeBlanc, S.; Asheghi, M.; Chen, B.; Goodson, K. E., Power density optimization for micro thermoelectric generators. *Energy* **2015,** *93*, 2006-2017.

12. Witting, I. T.; Chasapis, T. C.; Ricci, F.; Peters, M.; Heinz, N. A.; Hautier, G.; Snyder, G. J., The Thermoelectric Properties of Bismuth Telluride. *Advanced Electronic Materials* **2019,** *5* (6), 1800904.

13. Lal, S.; Gautam, D.; Razeeb, K. M., Optimization of annealing conditions to enhance thermoelectric performance of electrodeposited p-type BiSbTe thin films. *APL Materials* **2019,** *7* (3), 031102.

14. Snyder, G. J.; Toberer, E. S., Complex thermoelectric materials. *Nat Mater* **2008,** *7* (2), 105-114.

15. Sootsman, J. R.; Chung, D. Y.; Kanatzidis, M. G., New and old concepts in thermoelectric materials. *Angewandte Chemie* **2009,** *48* (46), 8616-39.

16. Liu, H.; Yuan, X.; Lu, P.; Shi, X.; Xu, F.; He, Y.; Tang, Y.; Bai, S.; Zhang, W.; Chen, L.; Lin, Y.; Shi, L.; Lin, H.; Gao, X.; Zhang, X.; Chi, H.; Uher, C., Ultrahigh Thermoelectric

Performance by Electron and Phonon Critical Scattering in Cu2Se1-xIx. *Advanced Materials* **2013,** *25* (45), 6607-6612.

17. Ge, Z.-H.; Zhang, B.-P.; Chen, Y.-X.; Yu, Z.-X.; Liu, Y.; Li, J.-F., Synthesis and transport property of Cu1.8S as a promising thermoelectric compound. *Chemical Communications* **2011,** *47* (47), 12697-12699.

18. He, Y.; Day, T.; Zhang, T.; Liu, H.; Shi, X.; Chen, L.; Snyder, G. J., High Thermoelectric Performance in Non-Toxic Earth-Abundant Copper Sulfide. *Advanced Materials* **2014,** *26* (23), 3974-3978.

19. He, Y.; Zhang, T.; Shi, X.; Wei, S.-H.; Chen, L., High thermoelectric performance in copper telluride. *Npg Asia Materials* **2015,** *7*, e210.

20. Qiu, P.; Shi, X.; Chen, L., Cu-based thermoelectric materials. *Energy Storage Materials* **2016,** *3* (Supplement C), 85-97.

21. Snyder, G. J.; Toberer, E. S., Complex thermoelectric materials. *Nature Mater* **2008,** *7*.

22. Pei, Y.; Shi, X.; Lalonde, A.; Wang, H.; Chen, L.; Snyder, G. J., Convergence of electronic bands for high performance bulk thermoelectrics. *Nature* **2011,** *473* (7345), 66-69.

23. Hinterleitner, B.; Knapp, I.; Poneder, M.; Shi, Y.; Müller, H.; Eguchi, G.; Eisenmenger-Sittner, C.; Stöger-Pollach, M.; Kakefuda, Y.; Kawamoto, N.; Guo, Q.; Baba, T.; Mori, T.; Ullah, S.; Chen, X.-Q.; Bauer, E., Thermoelectric performance of a metastable thin-film Heusler alloy. *Nature* **2019,** *576* (7785), 85-90.

24. Zhao, L.-D.; Dravid, V. P.; Kanatzidis, M. G., The panoscopic approach to high performance thermoelectrics. *Energy Environ. Sci.* **2014,** *7* (1), 251-268.

25. Yang, L.; Chen, Z.-G.; Dargusch, M. S.; Zou, J., High Performance Thermoelectric Materials: Progress and Their Applications. *Advanced Energy Materials* **2018,** *8* (6), 1701797.

26. He, R.; Schierning, G.; Nielsch, K., Thermoelectric Devices: A Review of Devices, Architectures, and Contact Optimization. *Advanced Materials Technologies* **2018,** *3* (4), 1700256.

27. Liu, W.; Kim, H. S.; Jie, Q.; Ren, Z., Importance of high power factor in thermoelectric materials for power generation application: A perspective. *Scripta Materialia* **2016,** *111*, 3-9.

28. Hatsuta, N.; Takemori, D.; Takashiri, M., Effect of thermal annealing on the structural and thermoelectric properties of electrodeposited antimony telluride thin films. *Journal of Alloys and Compounds* **2016,** *685*, 147-152.

29. Zhou, J.; Wang, H.; He, D.; Zhou, Y.; Peng, W.; Fan, F.; Huang, H., Transferable and flexible thermoelectric thin films based on elemental tellurium with a large power factor. *Applied Physics Letters* **2018,** *112* (24), 243904.

30. Gharavi, M. A.; Kerdsongpanya, S.; Schmidt, S.; Eriksson, F.; Nong, N. V.; Lu, J.; Balke, B.; Fournier, D.; Belliard, L.; le Febvrier, A.; Pallier, C.; Eklund, P., Microstructure and thermoelectric properties of CrN and CrN/Cr2N thin films. *Journal of Physics D: Applied Physics* **2018,** *51* (35), 355302.

31. Manzano, C. V.; Abad, B.; Munoz Rojo, M.; Koh, Y. R.; Hodson, S. L.; Lopez Martinez, A. M.; Xu, X.; Shakouri, A.; Sands, T. D.; Borca-Tasciuc, T.; Martin-Gonzalez, M., Anisotropic Effects on the Thermoelectric Properties of Highly Oriented Electrodeposited Bi2Te3 Films. *Sci Rep* **2016,** *6*, 19129.

32. Yan, X.; Poudel, B.; Ma, Y.; Liu, W. S.; Joshi, G.; Wang, H.; Lan, Y.; Wang, D.; Chen, G.; Ren, Z. F., Experimental Studies on Anisotropic Thermoelectric Properties and Structures of n-Type Bi2Te2.7Se0.3. *Nano Letters* **2010,** *10* (9), 3373-3378.

33. Pasquale, M. A.; Gassa, L. M.; Arvia, A. J., Copper electrodeposition from an acidic plating bath containing accelerating and inhibiting organic additives. *Electrochimica Acta* **2008,** *53* (20), 5891-5904.

34. Gabrielli, C.; Moçotéguy, P.; Perrot, H.; Nieto-Sanz, D.; Zdunek, A., An investigation of copper interconnect deposition bath ageing by electrochemical impedance spectroscopy. *Journal of Applied Electrochemistry* **2008,** *38* (4), 457-468.

35. Vazquez-Arenas, J.; Cruz, R.; Mendoza-Huizar, L. H., The role of temperature in copper electrocrystallization in ammonia–chloride solutions. *Electrochimica Acta* **2006,** *52* (3), 892-903.

36. Torrie, B. H., Raman spectrum of tellurium. *Solid State Communications* **1970,** *8* (22), 1899-1901.

37. Salmón-Gamboa, J. U.; Barajas-Aguilar, A. H.; Ruiz-Ortega, L. I.; Garay-Tapia, A. M.; Jiménez-Sandoval, S. J., Vibrational and electrical properties of Cu2−xTe films: experimental data and first principle calculations. *Scientific Reports* **2018,** *8* (1), 8093.

38. Dhasade, S. S.; Han, S. H.; Fulari, V. J., A nanostructured copper telluride thin film grown at room temperature by an electrodeposition method. *Journal of Semiconductors* **2012,** *33* (9), 093002.

39. Du, Y.; Qiu, G.; Wang, Y.; Si, M.; Xu, X.; Wu, W.; Ye, P. D., One-Dimensional van der Waals Material Tellurium: Raman Spectroscopy under Strain and Magneto-Transport. *Nano letters* **2017,** *17* (6), 3965-3973.

40. Carlos, R.-F.; Cristina, V. M.; Aldo, H. R.; Jaime, M.; Marisol, M.-G.; Mauricio Morais de, L., Jr.; Andrés, C., The fingerprint of Te-rich and stoichiometric Bi 2 Te 3 nanowires by Raman spectroscopy. *Nanotechnology* **2016,** *27* (7), 075706.

41. Martin, R. M.; Lucovsky, G.; Helliwell, K., Intermolecular bonding and lattice dynamics of Se and Te. *Physical Review B* **1976,** *13* (4), 1383-1395.

42. Yan, J.; Liao, X.; Yan, D.; Chen, Y., Review of Micro Thermoelectric Generator. *Journal of Microelectromechanical Systems* **2018,** *27* (1), 1-18.

Table of Contents (TOC)

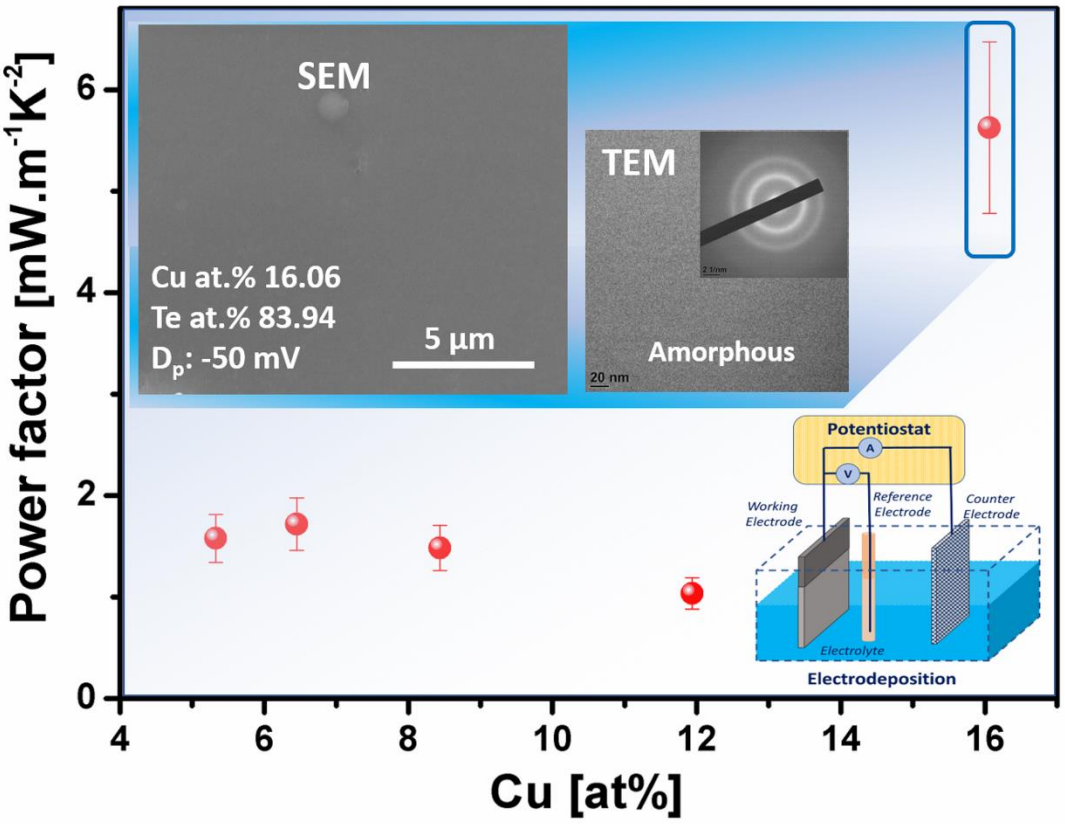

For Table of Contents Only